Mon. Not. R. Astron. Soc. **000**, 1–8 (2004) Printed 12 April 2004 (MN LATEX style file v2.2)

An Enlarged Cosmic Shear Survey with the William Herschel Telescope

Richard Massey,[1,2⋆] Alexandre Refregier,[3] David Bacon[4] and Richard Ellis[2]
[1] *Institute of Astronomy, Madingley Road, Cambridge CB3 OHA*
[2] *California Institute of Technology, Pasadena, California 91125, USA*
[3] *Service d'Astrophysique, CEA Saclay, F-91191 Gif sur Yvette, France*
[4] *Institute for Astronomy, Blackford Hill, Edinburgh EH9 3HJ*

Accepted —. Received —; in original form 8 April 2004.

ABSTRACT
We report the results of a cosmic shear survey using the 4.2m William Herschel Telescope on La Palma, to a depth of $R = 25.8$ ($z_s \approx 0.8$), over 4 square degrees. The shear correlation functions are measured on scales from $1'$ to $15'$, and are used to constrain cosmological parameters. We ensure that our measurements are free from instrumental systematics, by performing a series of tests including an E-B decomposition. We find that the normalisation of the matter power spectrum on 8 h^{-1}Mpc scales is $\sigma_8 = (1.09 \pm 0.12)(0.3/\Omega_m)^{0.51}$, with $\Omega_m > 0.25$, where the 68%CL error includes noise, sample variance, covariance between angular scales, systematic effects, redshift uncertainty and marginalisation over other parameters. We compare these results with other cosmic shear surveys and with recent constraints from the WMAP experiment.

Key words: cosmology: observations – gravitational lensing – large-scale structure of Universe.

1 INTRODUCTION

Weak gravitational lensing by large-scale structure, or "cosmic shear", has emerged as a powerful cosmological probe, as it is directly sensitive to foreground mass (for reviews, see Bartelmann & Schneider 2000; Bernardeau 1999; Mellier 1999; Refregier 2003; Wittman 2002). A measurement of cosmic shear is therefore closely tied to cosmological theories, which are principally concerned with the distribution of dark matter. In particular, the systematic biases of this technique are not limited by unknown physics such as biasing (Dekel & Lahav 1999; Gray et al. 2002; Hoekstra et al. 2002b; Smith et al. 2003; Weinberg et al. 2000) or the mass-temperature relation for X-ray selected galaxy clusters (Huterer & White 2003; Pierpaoli, Scott & White 2001; Viana, Nichol & Liddle 2002).

Cosmic shear surveys are rapidly growing in size and precision (Bacon et al. 2003; Brown et al. 2003; Hamana et al. 2003; Hoekstra et al. 2002a; Jarvis et al. 2003; Refregier Rhodes, & Groth 2002; Rhodes, Refregier & Groth 2001; Van Waerbeke et al. 2002). Cosmological parameter constraints from these surveys are now approaching the precision of other methods.

However, cosmic shear surveys can be subject to several systematic biases of their own. Imperfect telescope tracking, telescope flexure or optical misalignment within the camera, even at a level that is acceptable for most purposes, can artificially distort images and align the shapes of distant galaxies in a way that mimics cosmic shear.

The survey described in this paper represents a culmination of effort at the William Herschel Telescope. We have combined the experience of instrumentalists with detailed image simulations and careful data analysis to control the various sources of systematic error. Our first cosmic shear paper (Bacon, Refregier & Ellis 2000) reported an initial detection of cosmic shear using a 0.5 square degree survey with the William Herschel Telescope (WHT). The second paper (Bacon et al. 2003) compared the WHT shear signal with an independent measurement using the Keck II telescope, and examined systematics from these two very different instruments. In this paper, we extend our WHT survey to cover 4 square degrees to constrain cosmological parameters, while paying great care in monitoring and correcting systematic effects.

This paper is organised as follows. In §2 we describe our survey strategy and observational parameters. In §3 we present our results and draw constraints upon cosmological parameters. In §4 we test for the presence of any systematic errors. Assured that these are all negligible, we then conclude in §5.

⋆ E-mail: rjm@astro.caltech.edu

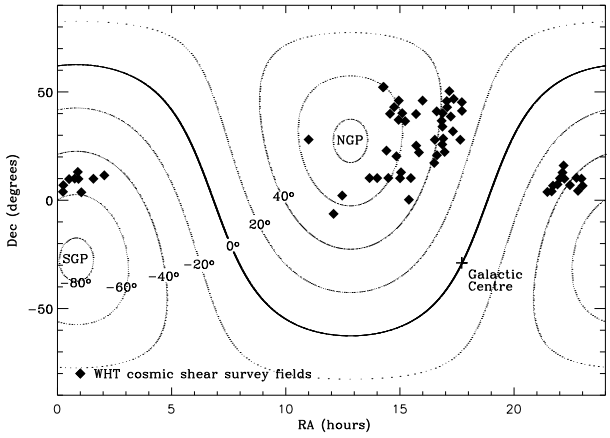

Figure 1. The locations of WHT pointings in our deep pencil-beam survey strategy. The galactic latitudes were tuned to provide sufficient foreground stars within each image to successfully model and correct for variations in the PSF.

2 OBSERVATIONS AND DATA REDUCTION

We have acquired 4 square degrees of imaging to $R = 25.8$ (for a point source at 5σ) with the *Prime Focus Imaging Camera* (PFIC) of the William Herschel Telescope on La Palma. The median seeing was $0.69''$ and no exposures had seeing worse than $1''$. The pixel size is $0.24''$. As shown in figure 1, pointings were scattered randomly in a pencil-beam survey between galactic latitudes of 30° and 70°. This was tuned to provide ~ 1.5 stars per arcmin^2, with which we could measure the Point Spread Function (PSF) across each field. The only selection criterion was to avoid foreground stars brighter than $R \approx 11$ in the Digitised Sky Survey or APM (Automated Plate Measuring machine) catalogues.

Cosmic shear statistics have already been presented from the first square degree of this survey in Bacon et al. (2003). That data consisted of eight $8' \times 16'$ images and eleven $16' \times 16'$ images taken after the addition of a second, identical CCD to the PFIC. During June and August 2002, we added an additional 41 $16' \times 16'$ pointings to this data set. The early, half-sized fields include fewer galaxy pairs on large scales than do the later, larger fields. The ideal way to weight their contributions is not clear; however, there are so few that any weighting scheme makes little difference to the final result, so, for simplicity, we weight them 1:2.

For each survey field we took four 900s exposures, each dithered by a few arcseconds from the last. This strategy enabled a continual monitoring of astrometric distortions within the telescope, cosmic ray removal, and lower overheads in the event of inclement weather. Data reduction then proceeded for the exposures exactly as in Bacon et al. (2003). After bias subtraction and flat fielding, fringing remained in the R-band images. This could have been prevented by observing at a shorter wavelength, but at a cost to the observed number density of background sources. To remove this, a fringe frame was compiled from all the exposures in each night. A multiple of this was subtracted from each image which minimised fringing, to a negligible level $< 0.05\%$ of the background noise. The four dithers for each field were then realigned (using linear interpolation between adjacent pixels to allow sub-pixel offsets) and stacked (with 3σ-clipping to remove cosmic rays).

Objects were located on the final images using HFINDPEAKS from the IMCAT package by Kaiser, Squires & Broadhurst (1995, KSB). Following the recommendations of Massey et al. (2001), objects within $10''$ of saturated stars or $5''$ of the edge of the CCDs were masked and removed. We also remove noisy objects from the catalogue with cuts in size, signal-to-noise and ellipticity of $r_g > 1$ pixel, $\nu > 15$ and $\varepsilon < 0.5$. After these cuts, 15 galaxies remained per arcmin^2, with a median magnitude of 23.5 ± 0.2. According to Cohen et al. (2000), this corresponds to a median source redshift of $z_s \simeq 0.80 \pm 0.06$. We fitted the moments of the PSF across the field using polynomial interpolation from the measured shapes of stars within each image. We then corrected every galaxy's shape for convolution with this PSF, and formed shear estimators γ using an implementation of the KSB method, including the calibration factor of $(0.85 \pm 0.04)^{-1}$ determined from simulated WHT images by Bacon et al. (2001).

Each set of four dithered exposures were also used to continually monitor astrometric distortions within the telescope. These were observed in Bacon et al. (2001) to closely follow the engineering predictions in the PFIC manual of $\gamma_{\rm tangential} = 0$, $\gamma_{\rm radial} = -8.2 \times 10^{-5} r^2$ with r measured in arcminutes from the field centre. This is already almost negligible but, to be safe, we subtract it from the final shear catalogues using the shear addition and subtraction operators in Bernstein & Jarvis (2002).

3 RESULTS

3.1 Shear-shear correlation functions

The power spectrum of the weak lensing shear is given by

$$C_\ell^\gamma \;=\; \frac{9}{16}\left(\frac{H_0}{c}\right)^4 \Omega_m^2 \int_0^{\chi_h} \left[\frac{g(\chi)}{D_A(\chi)}\right]^2 P\left(\frac{\ell}{r},\chi\right)\,{\rm d}\chi, \qquad (1)$$

where χ is a comoving distance; χ_h is the horizon distance; $D_A(\chi)$ is an angular diameter distance; $g(\chi)$ is the lensing weight function; and $P(k,z)$ is the underlying 3D distribution of mass in the universe. The shear correlations functions can be expressed in terms of the power spectrum as

$$C_1(\theta) \;=\; \frac{1}{4\pi}\int_0^\infty C_\ell^\gamma \left[{\rm J}_0(\ell\theta) + {\rm J}_4(\ell\theta)\right]\,\ell\,{\rm d}\ell \qquad (2)$$

$$C_2(\theta) \;=\; \frac{1}{4\pi}\int_0^\infty C_\ell^\gamma \left[{\rm J}_0(\ell\theta) - {\rm J}_4(\ell\theta)\right]\,\ell\,{\rm d}\ell\,. \qquad (3)$$

These can be measured by averaging over galaxy pairs, as

$$C_1(\theta) \;=\; \langle\, \gamma_1^r(\boldsymbol{r})\,\gamma_1^r(\boldsymbol{r}+\boldsymbol{\theta})\,\rangle \qquad (4)$$

$$C_2(\theta) \;=\; \langle\, \gamma_2^r(\boldsymbol{r})\,\gamma_2^r(\boldsymbol{r}+\boldsymbol{\theta})\,\rangle\,, \qquad (5)$$

where θ is the separation between the galaxies and the superscript ^{r} denotes components of shear rotated so that γ_1^r (γ_2^r) in the first galaxy points along (at 45° from) the vector between the pair. A third shear-shear correlation function can be formed,

$$C_3(\theta) \;=\; \langle\, \gamma_1^r(\boldsymbol{r})\,\gamma_2^r(\boldsymbol{r}+\boldsymbol{\theta})\,\rangle \;+\; \langle\, \gamma_2^r(\boldsymbol{r})\,\gamma_1^r(\boldsymbol{r}+\boldsymbol{\theta})\,\rangle\,, \qquad (6)$$

for which the parity invariance of the universe requires a zero signal. $C_3(\theta)$ can therefore be used as a first test for the presence of systematic errors in our measurement.

To perform the measurement in practice, we first measure the shear correlation functions for all galaxy pairs in one field and for several θ bins. To obtain a combined result for the entire survey, we then average the binned values for individual fields, with 3σ-clipping to remove outliers, and also excluding fields with similarly outlying values of $C_3(\theta)$ and of the star-galaxy cross-correlation functions $C_1^{SG}(\theta) + C_2^{SG}(\theta)$ (see §4.2). The result is shown in figure 2.

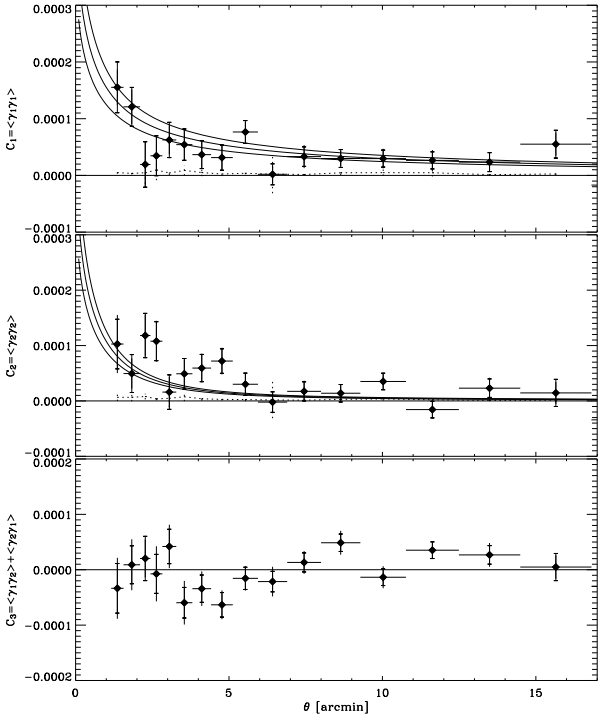

Figure 2. Correlation functions of the shear field measured in our 4 square degree WHT survey. The data points show our measurement. The inner error bars are for statistical errors only; the outer error bars also include full non-Gaussian sample variance. The solid lines are theoretical predictions for a ΛCDM cosmology with $\Omega_m = 0.3$, $\Omega_\Lambda = 0.7$, $\sigma_8 = 1$ and $\Gamma = 0.21$, calculated from equations (2) and (3), using the fitting functions of Smith et al. (2003), with a source redshift for all galaxies at $z_s = \{0.8, 0.9, 1.0\}$ from bottom to top, respectively. The dotted lines show the correlation of the galaxy shears with the (uncorrected) stellar ellipticity of the PSF (see §4.2).

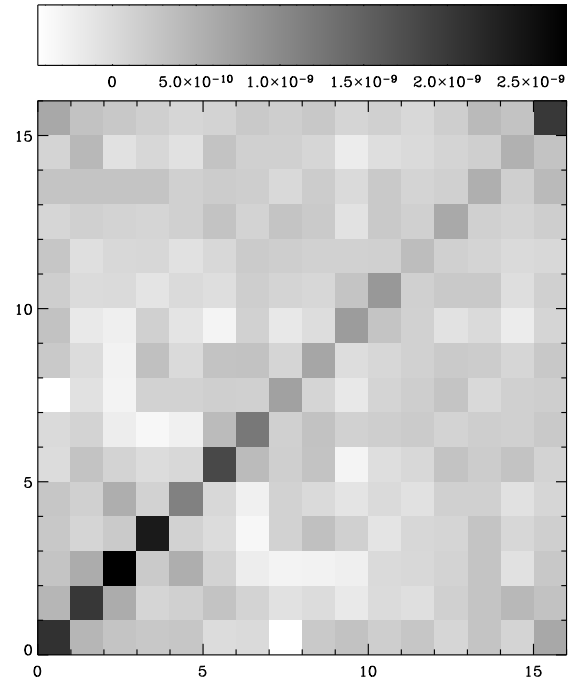

Figure 3. Covariance matrix of the different angular bins (labeled from 0 to 15) of the shear correlation functions shown in figure 2.

In order to derive constraints on cosmological parameters, it will also be necessary to know the covariance of $C_i(\theta)$ between different angular scales. Our pencil-beam survey strategy with many independent fields makes it easy to measure their covariance matrix

$$\mathrm{cov}[C_i(\theta), C_j(\vartheta)] \simeq \frac{1}{N_f^2} \sum_{f=1}^{N_f} \left[C_i^f(\theta) - C_j(\theta)\right] \left[C_i^f(\vartheta) - C_j(\vartheta)\right] , \quad (7)$$

where the summation is over all $N_f = 60$ fields, and the superscript ^{f} denotes correlation functions calculated in one field alone. This matrix is depicted in figure 3, and shows the significant covariance, especially between adjacent bins.

3.2 Cosmological parameter constraints

We now use a Maximum Likelihood method to determine the constraints set by our observations upon the cosmological parameters Ω_m, the total mass-density of the universe, and σ_8, the normalisation of the matter power spectrum at 8 h^{-1} Mpc. The analysis directly uses the observed correlation functions $C_1(\theta)$ and $C_2(\theta)$, proceeding as in Bacon et al. (2003), except that theoretical predictions are calculated via the fitting functions of Smith et al. (2003) rather than those by Peacock & Dodds (1996) which are less accurate. This has the effect of lowering our final constraint on $\sigma_8\Omega_m^{0.5}$ by about 5%. Note that, although we have performed an E/B decomposition, we fit C_1 and C_2 rather than the E mode alone to avoid degeneracies arising for the finite survey size. We will use the E/B decomposition a posteriori as a consistency check for systematics (see discussion in §4).

The theoretical correlation functions were first calculated from equation (1) on a 2D grid across the Ω_m–σ_8 plane. The median redshift for source galaxies was fixed to $z_s = 0.8$ for WHT and $z_s = 0.9$ for Keck, and the power spectrum shape parameter set to $\Gamma = \Omega_m h = 0.21$, consistent with recent observations of clustering in galaxy redshift surveys (Percival et al. 2001; Szalay et al. 2003). Errors on these parameters will be propagated separately into our final constraints. Because of contamination from systematic effects (see §4), we discarded the first and last data points from figure 2. We chose to double the size of the angular bins as compared to figure 2, as it yields tighter cosmological constraints; this is due to the significant covariance between the angular bins as shown in figure 3. We then fitted the observed shear correlation functions $\vec{d}(\theta)$ to the theoretical predictions calculated at the centres of each bin $\vec{t}(\theta)$, computing the log-likelihood function

$$\chi^2 = \left(\vec{d}(\theta) - \vec{t}(\theta, \Omega_m, \sigma_8)\right)^T \mathrm{cov}[C_i(\theta), C_j(\vartheta)] \left(\vec{d}(\vartheta) - \vec{t}(\vartheta, \Omega_m, \sigma_8)\right) \quad (8)$$

throughout the grid. We thus explore parameter space in this plane, and minimise χ^2 to find the best-fit cosmological model. To compute confidence contours, we numerically integrate the likelihood function

$$L(\Omega_m, \sigma_8) = e^{-\chi^2/2} . \quad (9)$$

Our constraints are presented in figure 4, and the constraints from our Keck survey (Bacon et al. 2003) are reproduced in the same format in figure 5. In both cases, the contours show 68.3%, 95.4% and 99.7% confidence limits, including statistical errors and non-Gaussian sample variance. They reveal the well-known de-

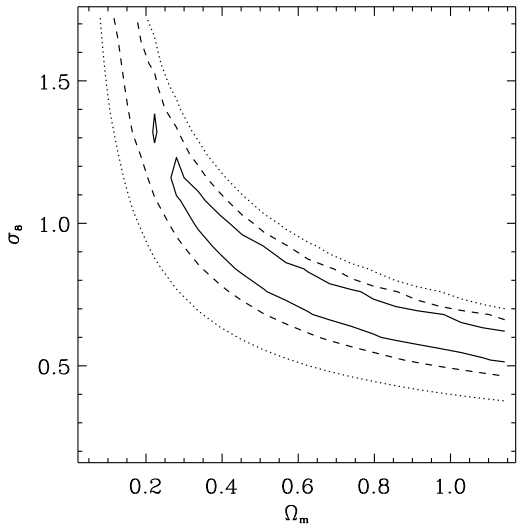

Figure 4. Constraints upon cosmological parameters Ω_m and σ_8, from a maximum-likelihood analysis of our WHT cosmic shear survey data. The 68.3% (solid), 95.4% (dashed) and 99.7% (dotted) confidence limits include statistical errors and non-Gaussian cosmic variance. However, they include neither the calibration of the shear measurement method, nor uncertainty in the source galaxy redshift distribution. These sources of error are considered separately in the text.

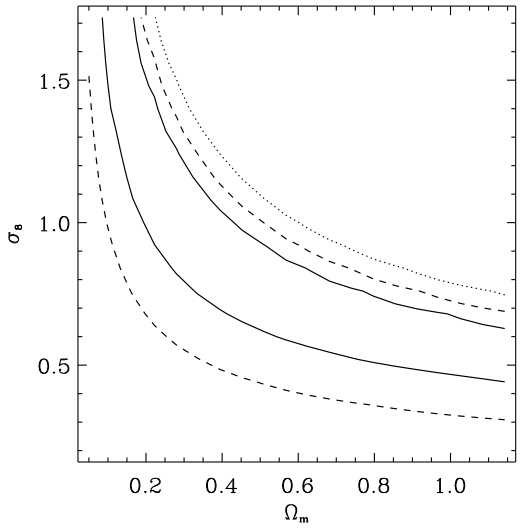

Figure 5. Constraints upon cosmological parameters from the Keck cosmic shear survey by Bacon et al. (2003), showing the 68.3%, 95.4% and 99.7% confidence limits as in figure 4. Only one edge of the 99.7% confidence contour is visible inside this parameter range.

generacy between Ω_m and σ_8 when using only two-point statistics, although the leverage created by the wide range of angular scales probed by our survey is beginning to exclude small values of $\Omega_m < 0.25$ (at 68%CL).

A good fit to the 68.3% confidence level from our WHT data is given by

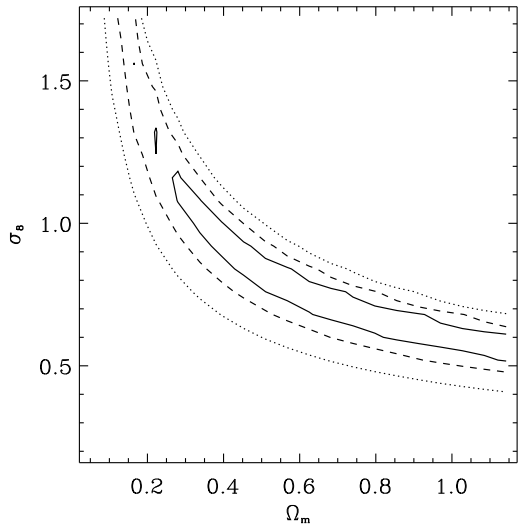

Figure 6. Constraints upon cosmological parameters for the combination of both WHT and Keck surveys, showing the 68.3%, 95.4% and 99.7% confidence limits, as in figure 4.

$$\sigma_8 \left(\frac{\Omega_m}{0.3}\right)^{0.52} = 1.11 \pm 0.10 \,, \tag{10}$$

for $0.25 < \Omega_m < 0.8$, while the Keck data is well-fit by

$$\sigma_8 \left(\frac{\Omega_m}{0.3}\right)^{0.52} = 1.01 \pm 0.19 \,, \tag{11}$$

The multiplication of the respective likelihood functions provides a constraint from a combined survey. Such confidence contours are shown in figure 6, with the 68.3% confidence level well-fit by

$$\sigma_8 \left(\frac{\Omega_m}{0.3}\right)^{0.52} = 1.09 \pm 0.09 \,, \tag{12}$$

for $0.1 < \Omega_m < 0.8$.

Note that all of these constraints include only the statistical error and sample variance. We can propagate other sources of error by noting that

$$C_i(5') \propto \Omega_m^{1.46} \sigma_8^{2.45} z_s^{1.65} \Gamma^{-0.11} (P^\gamma)^{-2}, \tag{13}$$

where $i = 1$ and 2 and P^γ is the shear calibration factor, in a fiducial ΛCDM cosmological model with $\Omega_m = 0.3$, Ω_Λ=0.7, $\Gamma = 0.21$ and $\sigma_8 = 1.0$. Adding in turn to our constraint (12): a 10% source redshift uncertainty, a 15% prior on Γ, and a 5% shear calibration uncertainty gives a final 68.3% CL constraint for the combined survey of

$$\sigma_8 \left(\frac{\Omega_m}{0.3}\right)^{0.52} = 1.09 \pm 0.09 \pm 0.073 \pm 0.007 \pm 0.044 \tag{14}$$

$$= 1.09 \pm 0.12 \,, \tag{15}$$

where the various errors have been combined in quadrature on the second line. This result now includes all contributions to the total error budget: statistical noise, sample variance, covariance between different angular scales, shear calibration error, source redshift uncertainty, and marginalisation over Γ.

3.3 Shear variance

For historical reasons, cosmic shear results are often expressed as the variance of the shear field in circular cells on the sky. For a top-

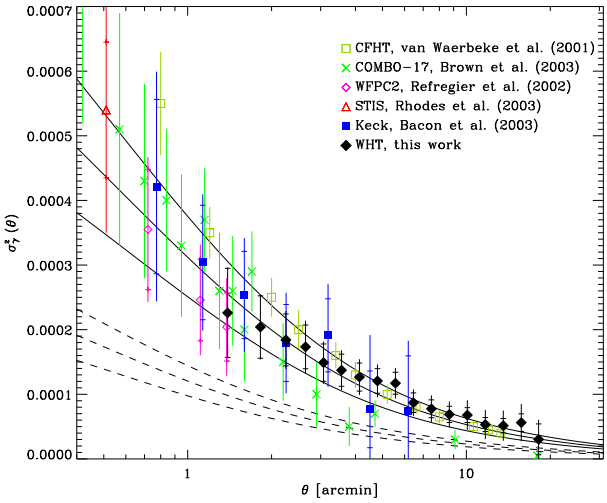

Figure 7. Shear variance in (circular, top-hat) cells, as a function of the radius of the cells. Our results are compared to those from similarly deep surveys by other groups (see text). The solid lines show the theoretical predictions, as before, for a ΛCDM model with $\Omega_m = 0.3$, Ω_Λ=0.7, $\Gamma = 0.21$ and $\sigma_8 = 1.0$, assuming a median source redshift of $z_s = \{0.8, 0.9, 1.0\}$ from bottom to top respectively, reflecting the dispersion in z_s in these different surveys. The dashed lines show theoretical predictions for the same three median source redshifts, but in a universe with $\sigma_8 = 0.7$, compatible with recent measurements of X-ray selected cluster abundances.

hat cell of radius θ, this measure is related to the shear correlation functions by

$$\sigma^2_\gamma \equiv \langle\, |\overline{\gamma}|^2 \,\rangle = \frac{2}{\pi}\int_0^\infty C^\gamma_\ell(\ell)\,\left[\mathrm{J}_1(\ell\theta)\right]^2\,\ell\,\mathrm{d}\ell \qquad (16)$$

$$\simeq \frac{2}{\theta^2}\int_0^\theta \left[C_1(\vartheta)+C_2(\vartheta)\right]\,\mathrm{d}\vartheta\,, \qquad (17)$$

where we have used a small angle approximation involving the Bessel functions. Note that the shear variance is more strongly correlated on different angular scales in this form than they are as correlation functions.

In practice, data is not available on all the scales necessary to perform this integration. The correlation functions have not been calculated on scales smaller than $1'$, and are contaminated by systematics on scales smaller than $2'$ (see §4). We determine the deficit in the measured values as a function of θ by extrapolating the data through these scales using the theoretical predictions given by the best-fit cosmological model determined in §3.2. This deficit ($\sim 2\times10^{-5}$ at $3'$ and 1×10^{-5} at $5'$) is then added back on to our measured data points.

We present our results as the variance of shear in cells, and compare them to those from similarly deep lensing surveys in figure 7. These surveys use data from 8.5 square degree VIRMOS-DESCART survey on the 3.6m CFHT by Van Waerbeke et al. (2002); the 1.25 square degree COMBO-17 survey on the 2.2m La Silla telescope by Brown et al. (2003); the 0.36 square degree Medium Deep Survey with the *Wide Field and Planetary Camera* on HST by Refregier Rhodes, & Groth (2002); 0.27 square degrees of random fields observed in parallel-mode with the *Space Telescope Imaging Spectrograph* (STIS) on HST by Rhodes et al. (2004); and the 0.6 square degree pencil-beam survey using the 10m Keck II telescope by Bacon et al. (2003). Most of these deep surveys appear to prefer a value of σ_8 around unity.

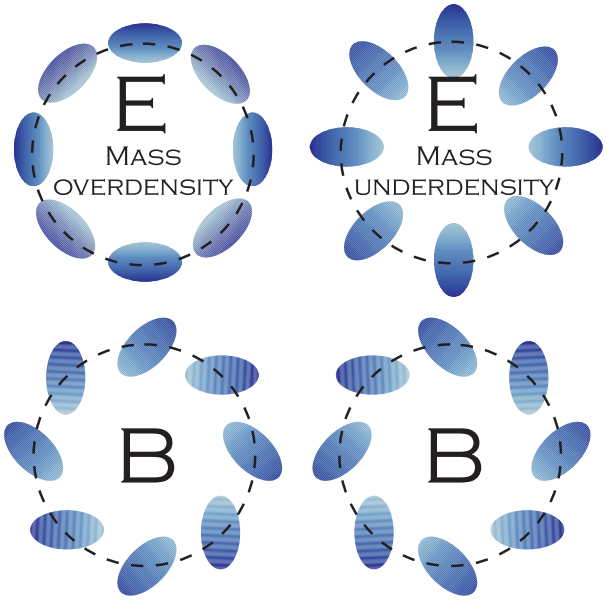

Figure 8. Gravitational lensing produces only E modes in the shear field. Gravitational lensing does not generally create B modes, and their presence can therefore be used as a diagnostic of systematic errors in observational data.

4 TESTS FOR SYSTEMATIC BIASES

The validity of any cosmic shear result depends sensitively upon the treatment of systematic errors and the control of observational biases. Almost all systematic effects, whether they be due to a background gradient, astrometric distortions within the telescope or imperfectly corrected PSF anisotropy, act to increase the observed correlations between galaxy shapes. All the effects can mimic cosmic shear and the most important task incumbent upon any weak lensing survey is to prove that its systematics are controlled to a negligible level. As already described in §2, the astrometric distortions in WHT have been corrected for, and the basic data reduction was performed sufficiently carefully to eliminate most biases. In this section, we discuss further tests for other sources of residual systematics.

4.1 E-B decomposition

The correlation functions can be recast in terms of E (gradient) and B (curl) modes of the shear field (Crittenden et al. 2000; Pen et al. 2002), as illustrated in figure 8. Gravitational lensing is expected to produce only E modes, except for a very low level of B modes due to lens-lens coupling along a line of sight (Schneider et al. 2002). It is commonly assumed that systematics effects would affect both E- and B-modes equally. The presence of a non-zero B mode would therefore be a useful indication of contamination from other sources.

E- and B-modes correspond to patterns within an extended region on the sky, and cannot be separated locally. As a result, this operation requires the integration of the shear correlation functions over a wide range of angular scales. In practice, we cannot perform the integrals exactly because our correlation function data extends only between $\sim 2'$ and $16'$. In other words, a given shear field within a finite aperture can not be uniquely split into distinct E- and B-mode components.

The aperture mass $M_{\rm ap}(\theta)$ provides a convenient and fre-

quently used method to separate the two components, by summing the tangential (γ_t) and radial (γ_r) components of shear relative to the centre of a circular aperture. The shears are weighted by a compensated filter $W(|\vec{\vartheta}|)$. Crittenden et al. (2000) showed that

$$M_{\rm ap}(\theta) \equiv \int_0^\infty W\left(|\vec{\vartheta}|;\theta\right)\ \gamma_t\left(\vec{\vartheta}\right)\ {\rm d}^2\vec{\vartheta} \tag{18}$$

contains only contributions from the E-mode signal and that

$$M_\perp(\theta) \equiv \int_0^\infty W\left(|\vec{\vartheta}|;\theta\right)\ \gamma_r\left(\vec{\vartheta}\right)\ {\rm d}^2\vec{\vartheta}\,, \tag{19}$$

contains only the B-mode signal. Schneider et al. (2002) derived expressions for the variance of these statistics using a compensated "Mexican hat" weight function

$$W(\vartheta;\theta) = \frac{6}{\pi\theta^2}\frac{\vartheta^2}{\theta^2}\left(1-\frac{\vartheta^2}{\theta^2}\right){\rm H}(\theta-\vartheta)\,, \tag{20}$$

where θ defines an angular scale of the aperture and the Heaviside step function H truncates the weight function at high scales. Following the notation of Crittenden et al. (2000), we first define $C_+ \equiv C_1 + C_2$ and $C_- \equiv C_1 - C_2$, then calculate

$$\left\langle M_{\rm ap}^2\right\rangle(\theta) = \frac{1}{2}\int_0^{2\theta}\frac{{\rm d}\vartheta\vartheta}{\theta^2}\left[C_+(\vartheta)T_+\left(\frac{\vartheta}{\theta}\right)+C_-(\vartheta)T_-\left(\frac{\vartheta}{\theta}\right)\right] \tag{21}$$

$$\left\langle M_\perp^2\right\rangle(\theta) = \frac{1}{2}\int_0^{2\theta}\frac{{\rm d}\vartheta\vartheta}{\theta^2}\left[C_+(\vartheta)T_+\left(\frac{\vartheta}{\theta}\right)-C_-(\vartheta)T_-\left(\frac{\vartheta}{\theta}\right)\right], \tag{22}$$

where

$$T_+(x) = \frac{6(2-15x^2)}{5}\left[1-\frac{2}{\pi}\arcsin\left(\frac{x}{2}\right)\right]\ + \tag{23}$$
$$\frac{x\sqrt{4-x^2}}{100\pi}\left(120+2320x^2-754x^4+132x^6-9x^8\right)$$

$$T_-(x) = \frac{192}{35\pi}x^3\left(1-\frac{x^2}{4}\right)^{7/2} \tag{24}$$

for $x < 2$ and $T_+(x) = T_-(x) = 0$ for $x \geqslant 2$.

Unfortunately, we find that these integrals are numerically unstable when performed upon binned data. The function $T_+(x)$ places a lot of weight upon the value of the correlation functions at small angular scales. Since this is changing rapidly, the end result is highly sensitive to the spacing of the bins. Furthermore, our measured correlation functions are least reliable at small separations, and are likely to be so in all real data at very small separations because of small-scale effects like overlapping galaxy isophotes. These small scales are included in all integrals, and a bias there would adversely affect $\langle M_{\rm ap}^2\rangle$ on all scales.

We shall therefore prefer to use another method for E/B decomposition based on the correlation functions. Following again Crittenden et al. (2000), we calculate

$$C_E(\theta) \equiv C_1(\theta) + 2\int_\theta^\infty\left(1-\frac{3\theta^2}{\vartheta^2}\right)\frac{C_-(\vartheta)}{\vartheta}\,{\rm d}\vartheta\,, \tag{25}$$

which contains only the E-mode signal and

$$C_B(\theta) \equiv C_2(\theta) - 2\int_\theta^\infty\left(1-\frac{3\theta^2}{\vartheta^2}\right)\frac{C_-(\vartheta)}{\vartheta}\,{\rm d}\vartheta\,, \tag{26}$$

which contains only the B-mode signal. The $C_E(\theta)$ and $C_B(\theta)$ have the advantage that the only missing data comes from large angular separations, where the expected signal (and the necessary correction) is small. As can be seen from the above equation, it is generally necessary to add a function of θ (not only a constant of integration) to $C_E(\theta)$ and subtract it from $C_B(\theta)$(c.f. Pen et al. 2002). We calculate this function by using theoretical predictions for the best-fit cosmological model (as determined in §3.2) to extrapolate our data to infinity. The size of this correction is approximately one third of the size of the measured E-mode signal. The correction is 2.4×10^{-5} at $5'$ and 1.5×10^{-5} at $10'$.

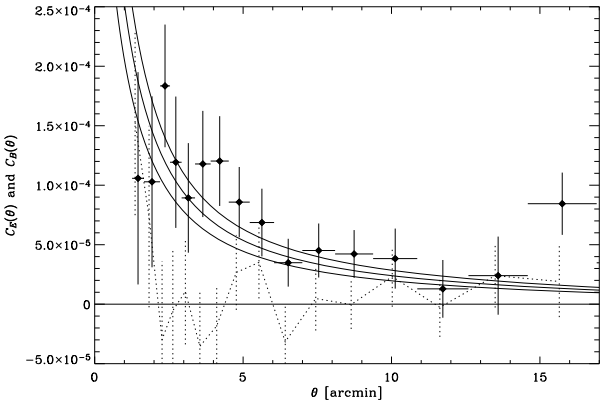

Figure 9. E-B decomposition of the shear field observed in our WHT survey. The points show the measured E (tangential) modes of the shear field. The solid lines show theoretical predictions for the E-modes for a ΛCDM model, with $\Omega_m = 0.3$, Ω_Λ=0.7, $\Gamma = 0.21$ and $\sigma_8 = 1.0$, assuming a median source redshift of $z_s = \{0.8, 0.9, 1.0\}$ from bottom to top respectively. The dotted line shows our measured B-mode (curl) signal which, in the absence of systematics, should be consistent with zero.

An E-B decomposition of our data is shown in figure 9. On scales $1.7' < \theta < 15'$, we find a B-mode signal consistent with zero, confirming the absence of systematics on these scales. Note that because of the extra uncertainty introduced by the additive function, we have not use the derived E-mode signal to fit cosmological parameters. We instead direcly fit the measurements of C_1 and C_2 on those scales deemed free of systematic errors (see §3.2).

4.2 PSF correction

The WHT PSF over long exposures can be quite anisotropic, with a mean stellar ellipticity of 0.051 ± 0.28, where the error quoted is the rms stellar ellipticity within one field, averaged over all fields. Application of KSB reduces this to 0.0056 ± 0.0012. However, uncertainties remain about the KSB correction and shear calibration (e.g. Bernstein & Jarvis 2002; Van Waerbeke et al. 2002). Detailed image simulations by Bacon et al. (2001) or Erben et al. (2001) have been used to study these issues; Bacon et al. (2001) found that, with our survey and telescope parameters, our implementation of KSB requires a constant calibration factor of $(0.85 \pm 0.04)^{-1}$ to all calculated shear estimators.

The correction for the PSF anisotropy can be tested using cross-correlation functions between corrected shears γ_i from galaxies and stellar ellipticity e_i^* before correction,

$$C_i^{\rm SG} \ \equiv\ \frac{\langle\,\gamma_i\ e_i^*\,\rangle^2}{\langle\,e_i^*\ e_i^*\,\rangle}, \tag{27}$$

where $i = \{1, 2\}$. These cross-correlation functions are shown as dotted line in the top two panels of figure 2, and is consistent with zero on all scales. Note that PSF correction residuals would also have appeared as B-modes in figure 9, which are instead consistent with zero.

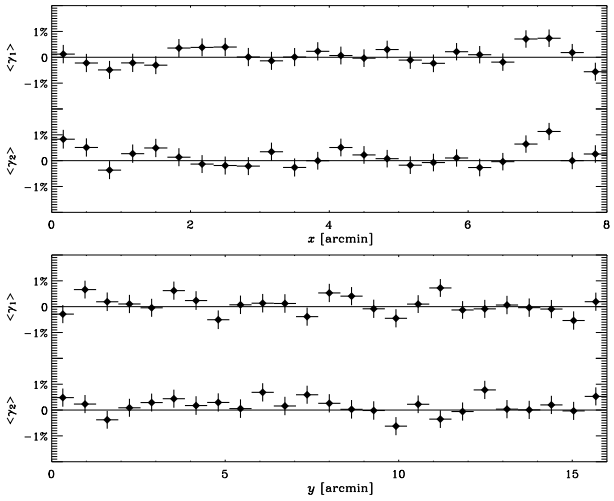

Figure 10. Galaxy shears as a function of position on the WHT CCD. When averaged over all the fields in our survey, this should be consistent with zero everywhere in the absence of systematics concerning CCD readout, telescope vibration and tracking.

4.3 Shear as a function of CCD position

Other systematics, including problems with read noise or charge transfer efficiency on the CCD and telescope flexure or vibration, could cause the shear to vary as a function of position on the chip, even when averaged over many separate fields. Figure 10 shows plots of shear as a function of x and y, which are consistent with zero.

The mean components of shear across the entire CCD are $\langle\gamma_1\rangle = (1.1 \pm 7.1) \times 10^{-4}$ and $\langle\gamma_2\rangle = (15.6 \pm 7.0) \times 10^{-4}$. After the catalogue cut at $\varepsilon < 0.5$, the rms shear within the survey is $\sigma_{\gamma_1} = 0.293$ and $\sigma_{\gamma_2} = 0.292$, or $\sigma_{|\gamma|} = \langle|\gamma|^2\rangle^{1/2} = 0.413$. The main, and irreducible, component of this value is the intrinsic ellipticity dispersion of source galaxies. From other work performed with high S/N space-based data (Rhodes et al. 2004; Refregier Rhodes, & Groth 2002) and simulations (Massey et al. 2004), we estimate a fundamental lower limit for this figure around 0.30.

5 DISCUSSION AND CONCLUSIONS

We have measured the weak lensing shear-shear correlation functions in four square degrees of deep R-band imaging data from the William Herschel Telescope. Our measurements constrain the amplitude of the mass power spectrum, $\sigma_8(\Omega_m/0.3)^{0.52} = 1.09 \pm 0.12$, including all contributions to the total 68%CL error budget: statistical noise, sample variance, covariance between different angular scales, systematic measurement and detection biases, source redshift uncertainty, and marginalisation with priors over other parameters. We have examined our data for contamination by systematic effects using a variety of tests including an E-B decomposition. These all demonstrate that the level of systematics in our data is consistent with zero.

Our measurement is at the relatively high end of the distribution of published cosmic shear results, but is consistent at the 1σ level with those from equivalently deep surveys by Van Waerbeke et al. (2002), Refregier Rhodes, & Groth (2002), and (Rhodes et al. 2004). Our results are also consistent within 1.5σ with CMB results from the Wilkinson Microwave Anisotropy Probe (WMAP) (Spergel et al. 2003).

These recent cosmic shear results are, however, discrepant at the 3σ level with measurements derived from the abundance of X-ray selected cluster samples based on an observational rather than theoretical mass-temperature relation (Borgani et al. 2001; Seljak 2001; Reiprich & Böhringer 2002; Viana, Nichol & Liddle 2002). These suggest $\sigma_8 \approx 0.75$. Amara & Refregier (2004) concluded that even extreme non-Gaussianity in the mass distribution would be insufficient to explain this discrepancy, because the two techniques probe similar mass scales. Further studies are therefore needed in both the cluster method, to understand the difference between the observed mass-temperature relation and that found in numerical simulations; and in the weak lensing method, to construct more reliable and better calibrated shear measurement methods. Such consistency checks will represent a crucial verification of the standard ΛCDM paradigm, so resolving this issue is of paramount importance.

The wide distribution of σ_8 constraints from recent cosmic shear surveys might also cast some aspersion upon their precision. For example, it might be argued that their dispersion largely arises from unknown or poorly-understood systematic effects. It is interesting to note that there is a possible trend in observed σ_8 with the depth of the survey. Results from the deep surveys discussed above appear to be 2–3σ higher than those from shallower surveys like Hoekstra et al. (2002a) and Jarvis et al. (2003). A similar value can also be obtained from Hamana et al. (2003), once account is taken of their observed B-modes. This discrepancy might arise from one of two sources. One possibility is the differences between the various shear measurement methods and selection cuts used in these separate analyses. It is possible that a further shear calibration factor ought to be applied to more of these methods, similar to the one adopted in this paper. The analysis of simulated images (with a known shear) has shown that the KSB method produces a particularly biased measurement of the shape of galaxies with low S/N (Bacon, Refregier & Ellis 2000). To improve the accuracy and agreement of future shape measurement methods, several independent techniques are currently being calibrated upon more realistic simulated images developed by Massey et al. (2004). A second possibility for the observed trend with survey depth is uncertainty in the redshift distribution of source galaxies in deep data. It is difficult to determine the precise redshift distribution of galaxies after excluding those smaller than a fixed apparent size. We have been conservative in this analysis and, as seen in equation (14), source redshift uncertainty is already a major component of our total error budget. However, the cosmic shear analysis of the deep multicolour COMBO-17 survey by Brown et al. (2003) could use photometric redshifts for nearly all objects, and did indeed obtain a comparatively low value for $\sigma_8(\Omega_m/0.3)^{0.49} = 0.72^{+0.08}_{-0.09}$. Of course, this one result could also be explained as sample variance, because the COMBO17 survey contains only four independent lines of sight. The resolution of these issues will require extensive spectroscopic follow-up and more accurate image simulations. Such advances are essential if the potential of the next generation of cosmic shear surveys is to be fully realised.

ACKNOWLEDGEMENTS

We thank Neil O'Mahony, Chris Benn and the WHT staff for their help with the observations. We thank Nick Kaiser for providing us with the IMCAT software, and to Douglas Clowe for advice on its

use. We thank Sarah Bridle and Jason Rhodes for useful discussions. DJB was supported by a PPARC postdoctoral fellowship.

REFERENCES

Amara A. & Refregier A., 2004, MNRAS submitted. astro-ph/0310345
Bacon D., Massey R., Refregier A. & Ellis R., 2003, MNRAS, 344, 673
Bacon D., Refregier A. & Ellis R., 2000, MNRAS, 318, 625
Bacon D., Refregier A., Clowe D. & Ellis R., 2001, MNRAS, 325, 1065
Bartelmann M. & Schneider P., 2000, Phys. Rep., 340, 291
Bernardeau F. 1999. *Proc. Cargese Summer Sch., Cargese, France*, ed. M Lachieze-Rey. astro-ph/9901117
Bernstein G. & Jarvis M., 2002, ApJ, 123, 583
Borgani S., Rosati P., Tozzi P., Stanford S., Eisenhardt P., Lidman C., Holden B., Della Ceca R., Norman C., Squires G., 2001, ApJ, 561, 13.
Brown M., Taylor A., Bacon D., Gray M., Dye S., Meisenheimer K. & Wolf C. MNRAS, 341, 100
Cohen J., Hogg D., Blandford R., Cowie L., Hu E., Songaila A., Shopbell P. & Richberg K., 2000, ApJ, 538, 29
Crittenden R., Natarajan P., Pen U.-L. & Theuns T., 2000, ApJ, 559, 552
Dekel, A. & Lahav, O., 1999, ApJ, 520, 24
Erben T., van Waerbeke L., Bertin E., Mellier Y. & Schneider P., 2001, A&A, 366, 717
Gray M., Taylor A., Meisenheimer K., Dye S., Wolf C. & Thommes E., 2002, ApJ, 568, 141
Hamana T. et al., 2003, ApJ in press, preprint astro-ph/0210450
Hämmerle et al., 2002, A&A, 385, 743
Huterer & White, 2003, ApJ, 578, L95
Hoekstra H., Yee H., Gladders M., Felipe Barrientos L., Hall P. & Infante, L., 2002a, ApJ, 572, 55
Hoekstra H., van Waerbeke L., Gladders M., Mellier Y. & Yee H., 2002b, ApJ, 577, 604
Jarvis M., Bernstein G., Fisher P., Smith D., Jain B. et al., 2003, AJ, 125, 1014
Kaiser N., Squires G. & Broadhurst T., 1995, ApJ, 449, 460
Massey R., Bacon D., Refregier A. & Ellis R., 2001, ASP conf. ser. Vol 283, p.193., eds. T. Shanks & N. Metcalfe.
Massey R. et al., 2004, AJ in press, preprint astro-ph/0304418
Massey R., Refregier A., Conselice C. & Bacon D., 2004, MNRAS, 348, 214
Mellier Y., 1999, ARA&A, 37, 127
Peacock J. & Dodds S., 1996, MNRAS, 280, 19
Percival W. et al., 2001, MNRAS, 327, 1297
Pen U., Van Waerbeke L. & Mellier Y., 2002, ApJ, 567, 31
Pierpaoli E., Scott D. & White M., 2001, MNRAS, 325, 77
Reiprich T. & Böhringer H., 2002, ApJ, 567, 716
Refregier A., 2003, ARA&A in press, preprint astro-ph/0307212
Refregier A., Rhodes, J. & Groth E., 2002, ApJL, 572, 131
Rhodes J., Refregier A. & Groth E., 2001, ApJL, 552, 85
Rhodes J., Refregier A., Collins N., Gardner J., Groth E. & Hill R., 2004, ApJ in press. astro-ph/0312283
Seljak U., 2001, MNRAS, 337, 769
Schneider P., van Waerbeke, L. & Mellier Y., 2002, A&A, 389, 729
Smith G., Edge A., Eke V., Nichol R., Smail I. & Kneib J.-P., 2003, AJ, 590, L79
Smith R., Peacock J., Jenkins A., White S., Frenk C., Pearce F., Thomas P., Efstathiou G. & Couchmann H., 2003, MNRAS, 341, 1311
Spergel D. et al. 2003, ApJS, 148, 175
Szalay A. et al. 2003, ApJ, 591, 1
van Waerbeke L., Mellier Y., Pelló R., Pen U.-L., McCracken H. & Jain, B., 2002, A&A, 393, 369
Viana P., Nichol R. & Liddle A., 2002, ApJ, 569,75
Weinberg D., Davé R., Katz N. & Hernquist L., 2003, ApJ submitted, preprint astro-ph/0212356
Wittman D. 2002. *Dark Matter and Gravitational Lensing, LNP Top. Vol.*, eds. F. Courbin, D. Minniti. Springer-Verlag. astro-ph/0208063

This paper has been typeset from a TEX/ LATEX file prepared by the author.